

## Investigation of Seismic Response of Cantilever Retaining Walls: Limit Analysis vs Shaking Table Testing

Panos Kloukinas

*Department of Civil Engineering, University of Bristol, U.K.*

Email address: [p.kloukinas@bristol.ac.uk](mailto:p.kloukinas@bristol.ac.uk)

Anna Scotto di Santolo

*Telematic University of Naples, Pegaso, Italy*

Email address: [anna.scottodisantolo@unipegaso.it](mailto:anna.scottodisantolo@unipegaso.it)

Augusto Penna

*Department of Civil Engineering, University of Sannio, Italy*

Email address: [apenna@unisannio.it](mailto:apenna@unisannio.it)

Matthew Dietz

*Department of Civil Engineering, University of Bristol, U.K.*

Email address: [m.dietz@bristol.ac.uk](mailto:m.dietz@bristol.ac.uk)

Aldo Evangelista

*Department of Civil and Environmental Engineering, University of Naples Federico II, Italy*

Email address: [evangeli@unina.it](mailto:evangeli@unina.it)

Armando Lucio Simonelli

*Department of Civil Engineering, University of Sannio, Italy*

Email address: [alsimone@unisannio.it](mailto:alsimone@unisannio.it)

Colin Taylor

*Department of Civil Engineering, University of Bristol, UK*

Email address: [colin.taylor@bristol.ac.uk](mailto:colin.taylor@bristol.ac.uk)

George Mylonakis\*

*Department of Civil Engineering, University of Bristol, UK*

*Department of Civil Engineering, University of Patras, Greece*

*Department of Civil and Environmental Engineering, UCLA, USA*

Email address: [g.mylonakis@bristol.ac.uk](mailto:g.mylonakis@bristol.ac.uk)

\*Corresponding author

0.90 Queens Building, University Walk, Clifton BS8 1TR

Telephone: +44 (0) 117 331 5838

## **Abstract**

The earthquake response of cantilever retaining walls is explored by means of theoretical analyses and shaking table testing conducted at University of Bristol (EERC - EQUALS). The theoretical investigations employ both limit analysis and wave-propagation methods, which take into account different aspects the problem such as inertia, strength, kinematics and compatibility of deformations. The experimental program encompasses different combinations of retaining wall geometries, soil configurations and input ground motions. The response analysis of the systems at hand aim at shedding light onto salient features of the problem, such as: (1) the magnitude of soil thrust and its point of application; (2) the relative sliding versus rocking of the wall base and the corresponding failure modes; (3) the importance of the interplay between soil stiffness, wall dimensions and excitation characteristics, as affecting the above. (4) the importance of wall dynamics and phase differences between peak stresses and displacements. The results of the experimental investigations are in good agreement with the theoretical models and provide a better understanding on the physics of the problem.

## **Keywords**

Retaining Walls, Seismic Earth Pressures, Soil-structure interaction, Model tests

## **1. Introduction**

Earth retaining walls are among the earliest and most common geotechnical structures. Despite the apparent simplicity of these systems, several aspects of their behavior are poorly understood, especially for conditions involving seismic action. Moreover, little progress has

been achieved in improving design methods, the basic aspects of which have been laid down over a century ago.

Despite a number of failures observed during post-earthquake investigations, it is recognized that the majority of retaining walls are over designed [1]. This may be attributed to: (a) conservative design approaches encompassing large safety factors, (b) overestimation of design actions, (c) underestimation of system resistances stemming from conservative selection of soil strength parameters, and (d) the beneficial effect of SSI mechanisms that is ignored in design.

With reference to design procedures, conservative global safety factors have been replaced in modern seismic codes and design provisions (e.g. the Eurocodes EC7 and EC8, the U.S. FEMA-NEHRP and AASHTO LRFD) by more rational Load and Resistance Factor Design (LRFD) approaches [1-4]. The associated partial factors take into account the uncertainties of load actions and the unfavourable variations of material parameters. The factored load combinations have to fulfil the capacity/demand ratios for a set of ultimate and/or serviceability limit states considered in the design.

Despite its known drawbacks, the classic pseudo-static Mononobe-Okabe (M-O) formula is still the main method proposed for the analysis of yielding walls. Various alternative formulations have been proposed in seismic codes and the literature, in addition to the M-O, to cover the inherent limitations of the method, by limit analysis and alternative wave propagation theories [1-11]. The validity of the pseudostatic M-O analysis has been criticised recently, following observations from shaking table and centrifuge tests, which indicate small variations in earth pressures for earthquake amplitudes up to 0.4g [12-14] in active conditions and 0.5g in passive [15]. The interpretation of the aforementioned studies indicates that pseudo-static seismic earth pressures and load combinations involving inertial forces are conservative, due to phasing issues [16]. Also, the earth pressure distribution was found to be closer to hydrostatic, contrary to the suggestions of the classical work by Seed & Whitman [17].

It is worth noting that, both the overestimation of the earth pressures and the underestimation of the system strength have also been interpreted as the effect of conservative selection of soil strength parameters, including the effect of cohesion which is generally neglected [18, 19]. A new interpretation of theoretical and experimental test results in the framework of kinematic soil-structure interaction has been recently presented by Brandenberg et al. [20].

In light of the foregoing, a better understanding of the behaviour of soil-wall systems and a more accurate estimation of the lateral earth pressures and pertinent load combinations appear desirable. In the ensuing, an analysis of cantilever retaining walls supported by spread footings is presented, based on the results of an exact limit stress solution [21-23]. Findings from the theoretical study are compared against observations from shaking table investigations of model walls. This paper complements and extends previous results reported by the authors [24-27]. It is emphasised that the theoretical investigations reported in the work at hand are restricted to limit analysis solutions. Extended numerical simulations based on finite-element and finite-difference analyses using non-linear constitutive models will be the subject of a future publication.

## **2. Theoretical background**

Reinforced concrete cantilever (“semigravity”) walls represent a popular type of retaining system which is widely considered as advantageous over conventional gravity walls, since it exploits the stabilizing action of the soil weight over the footing slab to improve stability.

The problem under consideration is depicted in Fig. 1: a sloping backfill ( $\beta$ ) of dry cohesionless soil having unit weight  $\gamma_s$  and friction angle  $\phi$ , is retained by a cantilever wall with unit weight  $\gamma_w$ , interface roughness  $\delta_w$  and dimensions  $H$  (stem height),  $\omega_1$ ,  $\omega_2$ ,  $t_t$  and  $t_b$ , (stem inclination angles and width),  $b_1$ ,  $b_2$ ,  $B$ , and  $t_f$ , (footing slab dimensions) and an embedment depth  $d_f$ . Under the combined action of gravity ( $g$ ) and seismic body forces ( $a_h \times g$ ) and ( $a_v \times g$ ) in the horizontal

and vertical direction, respectively, resulting to the pseudo-dynamic seismic angle  $\psi_e = \tan^{-1}[a_h/(1-a_v)]$ , the stress limit state of the backfill can be analysed by means of the uniform Rankine tensor of Fig 2a. Indeed, following the *infinite slope* assumption, which is asymptotically exact at large distances from the wall, the normal and shear stress acting at planes parallel to soil surface are determined as functions of depth  $z$ , providing a constant obliquity ratio  $\tau_\beta/\sigma_\beta = \tan(\beta + \psi_e)$  [21, 28-29]. This is evident from the position of the stress point  $(\sigma_\beta, \tau_\beta)$  on the Mohr circle. Accordingly, the pole of the Mohr circle is determined from geometry, facing the stress point at an angle equal to the slope inclination,  $\beta$ . Since the position of the pole is known, the stresses acting on every plane can be established from trigonometry, based on the known stress point  $\sigma_\beta = \gamma z (1-a_v) \cos\beta \cos(\beta + \psi_e)/\cos\psi_e$ , by means of the auxiliary Caquot angle  $\Delta_{1e} = \sin^{-1}[\sin(\beta + \psi_e)/\sin\phi]$ .

As can be seen in Fig. 2b, when the stress characteristics do not intersect the stem of the wall (Eq.1), the aforementioned Rankine stress field is not affected by the roughness of the soil-wall interface. Given that the inclination of the stress characteristic  $\omega_\beta$  (Eq. 2) depends on acceleration level, the Rankine condition is valid for the vast majority of cantilever wall configurations under strong seismic action.

$$\omega_\beta \leq \omega_{cr} = \tan^{-1}(b_1/H + \tan\omega_1) \quad (1)$$

$$\omega_\beta = \frac{\pi}{4} - \frac{\phi}{2} - \frac{(\Delta_{1e} - \beta)}{2} - \frac{\psi_e}{2} \quad (2)$$

The traditional approach for analysing the system, is to assume that the soil thrust is acting on a conceptual vertical surface AD (Fig. 2b) passing through the innermost point of the wall base – the familiar vertical virtual back. Although the soil thrust can be evaluated on any arbitrary plane inclined at an angle  $\omega$ , the use of the vertical virtual back AD (i.e. choosing  $\omega = 0$ ) results to a simple geometry and equilibrium equations [30]. A contradictory issue in the literature relates to the selection of a proper mobilized obliquity on the AD plane, ranging, naturally, from

0 to  $\phi$  [30, 31]. Modern regulations recommend using Rankine conditions ( $\delta = \beta$ ) for long heel walls – for the condition of Eq. (2) and  $\delta$  equal to the natural wall roughness,  $\phi/3 \leq \delta_w \leq 2\phi/3$ , in the case of short heel walls [1]. These recommendations are clearly inadequate as demonstrated below.

Based on the seismic Rankine field of Fig 2a, exact closed-form solutions can be derived for the earth pressure coefficient  $K_{AE}$  (Eq. 3) by integrating the contact stresses ( $\sigma_0, \tau_0$ ) acting on the vertical plane, and the corresponding inclination of the soil thrust  $\delta(0)$  (Eq. 4), which is expressed by the ratio  $\tau_0/\sigma_0$  [23]. Equivalent stress limit analysis results have been derived, in a somewhat different form, by Evangelista et al. [21]. The robustness of the above stress limit analysis becomes evident since under the mobilized inclination  $\delta(0)$ , the Rankine and the Mononobe-Okabe solutions (both involving planar failure surfaces) coincide, as has already been observed for the gravitational case [30, 32].

$$K_{AE} = \frac{\cos \beta \cos(\beta + \psi_e)}{\cos \delta(0) \cos \psi_e} \left[ \frac{1 - \sin \phi \cos(\Delta_{1e} - \beta + \psi_e)}{1 + \sin \phi \cos(\Delta_{1e} + \beta + \psi_e)} \right] \quad (3)$$

$$\delta(0) = \tan^{-1} \left[ \frac{\sin \phi \sin(\Delta_{1e} - \beta + \psi_e)}{1 - \sin \phi \cos(\Delta_{1e} - \beta + \psi_e)} \right] \quad (4)$$

Similarly to the inclination of the characteristic angle  $\omega_\beta$  of the seismic Rankine field, the mobilized thrust obliquity  $\delta(0)$  varies with earthquake acceleration. This variation is depicted in Fig. 3, by means of a numerical example for various slope inclinations and for soil friction angles  $\phi = 30^\circ$  and  $40^\circ$ . It is evident from the graph that  $\delta(0)$  ranges from the slope inclination  $\beta$  (for gravitational loading,  $\psi_e = 0$ ) to the maximum value  $\phi$  (for acceleration levels that correspond to a vertical characteristic,  $\omega_\beta = 0$ ). Numerical results confirming the variation of  $\delta(0)$  during dynamic excitation have been presented by the authors [21, 22].

In light of the above developments, the conventional pseudo-static analysis of cantilever walls is modified according to the free body diagram of Fig. 4. Note that despite the presence of the

vertical component of seismic action in the diagram, this loading is usually neglected in design, since the vertical motion is considered to have a minor effect on the response of elastoplastic systems such as the one at hand [33]. As can be seen from the graph, the Rankine solution is strictly applicable to plane AD, whereas the active earth pressure on the vertical face of the footing slab, AE, is considered to act under an inclination  $\delta_w$ . For convenience, the Rankine solution can be extended to the whole vertical back ED [21]. The same inclination  $\delta_w$  can be applied for the passive resistance on the left end of footing, which, however, is often neglected for ordinary pad foundations, in the absence of significant embedment depth or a footing key [1, 2].

The contact and body forces acting on the system are resisted upon the reactions  $H_d$  and  $V_d$  acting on the foundation slab. The combination of these two actions, together with the resulting eccentricity  $e$ , determines the bearing demand of the wall foundation, in the context of classical limit analysis procedures for a strip footing subjected to an eccentric inclined load [2].

The seismic Rankine analysis reveals a beneficial mechanism for the system stability, which decreases the horizontal thrust and increases the vertical contact force during the earthquake. In the numerical example of Fig. 5, the performance of the different assumptions for the inclination  $\delta$  is compared for the case of a rough wall ( $\delta_w = 2\phi/3$ ) retaining loose horizontal backfill ( $\beta=0^\circ$ ,  $\phi = 30^\circ$ ) in terms of horizontal and vertical component of the soil thrust and the resultant moment with respect to the footing centroid, which is important for the reaction eccentricity. More specifically, the horizontal and vertical components of total soil thrust  $P_{AE}$  are compared in Figs. 5a,b and the corresponding counterparts of the seismic increment  $\Delta P_{AE}$  are compared in Figs. 5c,d. It should be noted that in case of a varying inclination  $\delta(0)$ , the conventional “seismic increment” approach ( $\Delta P_{AE} = P_{AE} - P_A$ ) cannot be employed directly, since the vectors  $P_{AE}$ ,  $P_A$  are not co-axial, but can only be defined on the horizontal and the vertical components separately. In Fig. 5e, the seismic increment  $\Delta M_{AE}$  of the overturning

moment produced by the soil thrust is presented, normalised by the corresponding gravitational moment  $\Delta M_A$ ; in Fig. 5f the moment due to the total thrust  $M_{AE}$  is presented, normalised by the exact Rankine analysis value  $M_{AE, Rankine}$ .

It is evident from the graphs that the exact Rankine analysis [i.e., either Rankine or M-O with  $\delta = \alpha(0)$ ] results in a smaller increase of the horizontal seismic component and a greater increase of the vertical, respectively, compared to the established assumptions. This is causing a decrease of the moment produced from the soil thrust, as can be seen in fig. 5e (negative  $\Delta M_{AE}$  values). The gravitational “Rankine” assumption (M-O analysis with  $\delta = \beta = 0^\circ$ ) is too conservative, as it overestimates the horizontal component of soil thrust and underestimates the corresponding vertical component. In terms of the resultant moment, the overestimation approaches 100% for an acceleration level of 0.3g. On the other hand, the “Coulomb” assumption (M-O analysis with  $\delta = 2\phi/3$ ), is less conservative at high accelerations, but underestimates the overturning moment produced by the total soil thrust at low accelerations by 40% or so, for the gravitational case. Note however, that these deviations tend to decrease with increasing friction angle and slope inclination.

### ***2.1 Design optimization issues***

Stability analysis of retaining walls requires solving the problem of a surface footing designed against sliding and bearing capacity under rather unfavourable conditions (unilateral kinematics, inclined and eccentric loads, no surcharge). In most seismic codes and design specifications, the limit state against overturning - toppling is also specified on the basis of uplifting and rotation of the footing about the toe O. The conventional approach of taking the ratio of stabilizing and overturning moments is known to be misleading [34] and has been replaced by the control of eccentricity of the factored actions under the limits  $B/3$  [2] or  $B/3$  and  $8\sim 9B/20$  for foundations on soil and rock respectively [1].



For foundations on compliant soil, overturning is clearly not the critical failure mechanism as local bearing capacity failure under the wall toe precedes overturning, resulting to permanent rotation [35]. Design regulations specify that sliding-type failure can be acceptable under serviceability limits, but permanent rotation should be limited below 1/500 [1, 2]. Along the same lines, replacement of the overturning limit state by a proper bearing capacity check under more strict eccentricities limits of B/6 and B/4 for foundations on soil and rock, respectively, has been proposed [36].

## 2.2 Design optimization example

Design of a cantilever wall system can be optimized for different design acceleration levels  $a_{hd}$ , to provide economical designs under pre-specified safety factors [37]. The equations from the pseudostatic analysis of Fig. 4 are programmed in dimensionless form and the optimization is performed by finding the minimum wall cross sectional area under the restrictions:  $b_1/H \geq \omega_R - \omega_1$  (to ensure Rankine conditions),  $SF_{bear. capacity} = R_d/V_d \geq 1$  (to avoid bearing capacity failure),  $t_1/H \geq 0.035$ ,  $t_f = t_b/H \geq 0.1$  (minimum values from sizing rules),  $b_2/H$ ,  $\omega_1$ ,  $\omega_2 > 0$ . In addition, the embedment depth  $d_f$  was set equal to the footing thickness  $t_f$  and the safety factor against sliding,  $S_d/H_d$ , was left unrestricted. Ultimate sliding and bearing capacity resistances  $S_d$  and  $R_d$  were calculated with EC7 formulae, without employing partial safety factors [2].

The parameters of the numerical example shown in Fig 6 are: soil friction angle  $\phi = 35^\circ$  (both for backfill and foundation soil), relative wall-soil density  $\gamma_s / \gamma_w = 0.8$ , backfill slope  $\beta = 10^\circ$  and wall roughness  $\delta_w = 2\phi/3$ . The safety factor against bearing capacity was always maintained above 1, and the one corresponding to sliding is reduced according to Fig. 6a. In Figs 6b and 6d, the optimized ratios  $b_1/H$ ,  $b_2/H$  and the corresponding safety factors of the optimized geometry for gravitational conditions, are plotted as function of design acceleration. Evidently, safety against bearing capacity failure improves drastically, mainly because of the increase in

both  $b_1/H$  and  $b_2/H$ . On the other hand, sliding resistance is slightly improved with  $b_1/H$ , increasing both actions and resistances. Finally, Fig. 6c demonstrates that bearing capacity failure takes place under decreasing eccentricities (which are much lower than the EC8 and AASHTO limits), with increasing design acceleration. This highlights the sensitivity of the retaining wall designs to bearing capacity considerations.

### **3. Shaking table experimental investigation**

To resolve the above theoretical issues, a series of shaking table tests were conducted at the 6-DOF Earthquake Simulator of the Earthquake and Large Structures Laboratory (EQUALS) at the University of Bristol, UK. Despite some known difficulties related to scaling of the friction angle  $\phi$ , shaking table testing is in extensive use in earthquake geotechnical engineering practice for understanding failure mechanisms and verifying design hypotheses [38].

The experimental program encompassed testing on scaled wall models on a compliant base under different retaining wall geometries and input ground motions. The physical models were constructed in the large Equivalent Shear Beam container of EQUALS, with inner dimensions  $4.80m$  long,  $1m$  wide and  $1.15m$  deep, which is designed to match the shear stiffness of the contained soil and ensure plane strain conditions [39, 40].

#### ***3.1 Shaking table model geometry and instrumentation***

The model geometry adopted in the design, shown in Figure 7, had to take into consideration the container dimensions and the restrictions of the shaking table regarding the maximum payload. A maximum soil height of  $1m$  was selected, corresponding to a backfill of  $0.6m$  (equal to the wall height,  $H$ ) and a foundation soil layer of  $0.4m$  (equal to wall footing width,  $B$ ). The length of the retained backfill was selected at 5 times its height, whereas the corresponding free length in the front of the wall was 3 times the wall height. These distances were deemed

sufficient to eliminate the boundary effects and ensure free field conditions.

Three basic types of instruments were employed for the measurement of accelerations, displacements and strains, as shown in Figure 7. Twenty one (21) uniaxial accelerometers were used to monitor the motion of the shaking table, the shear stack and the wall-soil system, with the main area of interest being the wall itself, the retained soil mass and the free field. Four (4) LVDT transducers were used to measure the transient and permanent displacements of the wall. Additionally, thirty two (32) strain gauges were attached along the stem and the base of the wall, on three different cross sections, to monitor the bending of the wall. Lastly, non-contact displacement transducers were employed to monitor the backfill settlement, but proved to be inefficient due to low operational range ( $\sim 10\text{mm}$ ) and were replaced by a grid of coloured sand (see Fig. 12).

### ***3.2 Wall models and soil material properties***

The retaining wall model, depicted in Fig 8, was made of aluminium alloy 5083 plates with unit weight  $\gamma = 27 \text{ kN/m}^3$ , Young's modulus  $E = 70\text{GPa}$  and Poisson's ratio  $\nu = 0.3$ . A central wall segment of  $600\text{mm}$  width was created by two  $1\text{mm}$  thick vertical slits penetrating  $400\text{mm}$  down into the stem, to ensure plane strain response unaffected from possible boundary effects. Along the same lines, the base of the wall was subdivided into four  $240\text{mm}$ -wide aluminium segments, each secured to the wall stem with three M12 bolts.

A thickness of  $32\text{mm}$  was selected for all aluminium plates, following the criterion to keep bending deformations close to the lowest operational level of the strain gauges [ $\varepsilon_a = M_d t / 2 D_w \sim 10^{-5}$ , where bending stiffness  $D_w = E_w t^3 / 12(1 - \nu_w^2)$ ], to simulate a relatively rigid wall. Despite stiffening measures, the relative wall-soil flexibility parameter  $d_w = GH^3 / D_w$  [41] attained values of approximately 15 to 25, corresponding to a somewhat flexible wall.

### ***3.3 Soil material properties***

Both the backfill and the foundation soil layer consisted of dry, yellow Leighton Buzzard 14 – 25 (Fraction B) silica sand at different compaction levels. The specific soil material has been used extensively in experimental research and a wide set of mechanical and dynamic properties is available in the literature [42, 43]. The soil configuration consists of a dense supporting layer and a medium dense backfill. The base layer was formed by pouring sand in layers of *150-200 mm* thickness from a deposition height of 0.6m, and then densifying by strong shaking. The backfill was formed by pouring sand from a height of 200mm, to minimise the densification effect of the downward stream of sand without further densification. The soil material properties are summarised in Table 1. Based on the densities calculated for the soil layers, the peak friction angles were estimated empirically at  $42.5^\circ$  and  $33.5^\circ$ , for the foundation layer and the backfill, respectively [42].

The importance of keeping soil density low during testing under 1-g conditions is discussed in [40]. It is well known that a very loose soil mass is sensitive to dynamic condensation during seismic excitation. However, this mechanism was shown to have minor effect on the system response, for the following reasons: (a) the foundation layer was relatively dense, (b) the backfill was replaced following each strong shaking test series, (c) the soil material consists of uniform coarse grained sand with rounded grain shapes and is, thereby, less sensitive to dynamic compaction.

In addition to the soil properties, the mechanical properties of the interfaces are important for the soil-wall system behaviour [44, 45]. Two kinds of footing interfaces were employed: a) a smooth interface between an aluminium plate and soil; b) a rough interface created by pasting rough sandpaper on the footing surface. The interface friction angles were measured directly on the model via static pull tests. The resulting values are  $\delta_w = 23.5^\circ$  for the smooth (aluminium - soil) soil-wall interface and  $\delta_w = 28.5^\circ$  for the corresponding rough one (sandpaper - soil).

### **3.4 Model Configurations**

Three different model configurations (No1, No2 and No3) were tested: (a) Configuration No1, corresponding to the reference geometry of Fig. 2 ( $B=400\text{mm}$ ,  $b_1=300\text{mm}$ ,  $b_2=70\text{mm}$ ), with a smooth footing interface, (b) Configuration No2, corresponding to a shorter footing width ( $B=280\text{mm}$ ,  $b_1=250\text{mm}$ ,  $b_2=0$ ) and (c) Configuration No3, with an identical geometry as Configuration No2, but with a rough interface, as explained above.

The equilibrium characteristics of these configurations, as estimated based on the pseudo-static analysis of Fig. 4, are summarised in Table 2. It is evident that the above configurations induce different responses ranging from a sliding-sensitive wall (Configuration No1), to a rotationally sensitive one mobilizing a bearing capacity failure mechanism (Configuration No3). Configuration No2 represents an intermediate case having comparable safety factors against sliding and bearing capacity. From Table 2, it is also evident that the safety factor against bearing capacity is dramatically decreased with increasing acceleration compared to the corresponding safety factor against sliding.

## **4. Experimental procedure**

The three wall configurations were subjected to the following series of dynamic tests: (1) Exploratory white noise testing to investigate the soil-wall system response; (2) Harmonic-sinusoidal inputs at various excitation frequencies and increasing amplitude, until yielding of the wall and sufficient plastic deformation of the system is recorded; (3) Dynamic excitation of the system with scaled earthquake signals of increasing amplitude, until sufficient yielding of the wall is recorded. Note that restoration of the wall-backfill system was needed after steps 2 and 3.

During exploratory white noise testing, a random noise signal of bandwidth  $1-100\text{ Hz}$  and *RMS*

acceleration =  $0.005g$  was employed. Harmonic excitation involved sine dwells consisting of 15 steady cycles, 5-cycle ramp up to full test level at the beginning and a 5-cycle ramp down to zero at the end, to smoothen out the transition between transient and steady-state response. After dynamic investigation of the system at various excitation frequencies and low acceleration amplitude of  $0.05g$ , a sole frequency of  $7Hz$  was employed with increasing amplitude, until failure.

For the seismic testing, a modified version of the Sturmo record from the Irpinia-Italy, 1980 earthquake ( $M_w=6.9$ ,  $PGA=0.32g$ ), was selected, characterized by a strong motion duration of  $16.2sec$  and an energy transfer to a wide range of frequencies from  $0.1$  to  $3 Hz$  (predominant frequency of  $0.4 Hz$ ), as shown in Fig. 9. A frequency scale factor of 5 was applied to the original signal, according to scaling laws for 1-g conditions [46]. The frequency-scaled signal was applied starting at a low acceleration amplitude of  $0.05g$ , which was increased until failure. The excitation frequencies for both sinusoidal and seismic inputs were essentially pseudo-static, as they are much below the resonant frequencies of the system. Regarding the data acquisition, the output signals were filtered with a low pass Butterworth filter of  $80 Hz$  and sampled at  $1024 Hz$ , except of the white noise tests which were sampled at  $256 Hz$ .

## **5. Experimental results - discussion**

### ***5.1 Dynamic properties***

The estimation of the dynamic properties of the soil-wall system was based on the interpretation of the white noise test results in the context of established empirical correlations for soil stiffness [47] and the predictions of wave propagation theory. In Fig. 10, characteristic frequency response functions (FRF) for Configurations No1 and No3 are presented for the response of the wall, before and after the placement of the backfill, as well as for the backfill itself. Regarding the wall stem response (sensors A5 – A6), a frequency of  $25.5Hz$  measured

for Configuration No1 corresponds to the first vibration mode of a fixed base cantilever with the same stiffness and inertial properties. On the other hand, due to foundation rocking in Configuration No3, the fixed-base vibration mode of the cantilever cannot be mobilised, and a lower resonance frequency of  $19\text{Hz}$  is recorded. When the response of the wall with respect to the input acceleration is examined (sensors A1 – A6), these values reduce to  $23.5\text{ Hz}$  and  $17\text{ Hz}$ , respectively, reflecting the effect of the compliant base.

When the backfill is added, resonant frequencies of  $36$ ,  $47$  and  $52\text{ Hz}$ , appear (sensors A1 – A15). From them, the frequency of  $47\text{Hz}$  is identified as the fundamental natural frequency of the backfill, as back-calculated shear modulus at low strain  $G_0 = 16\rho H^2 f = 20\text{GPa}$  is compatible to the predictions of the empirical relation by Hardin & Drenvich [47], evaluated at the middle of the soil column. With the overburden stress of the backfill taken into account, the same correlation for the foundation layer yields  $G_0$  values of about  $40\text{GPa}$ . Based on these values, a resonant frequency of  $36\text{ Hz}$  is derived by means of 1D wave propagation theory for a two-layer medium [48], which is in good agreement with the frequencies recorded during white-noise testing. Finally, because of the finite length of the backfill (length to height ratio  $L/H \sim 5$ ) the corresponding resonant frequency increases from  $47\text{Hz}$  to  $52\text{ Hz}$  [11, 49]. This is essentially an indication of the stiffening effect of the box boundary. A summary of the above model parameters is presented in Figure 11. Additionally, the Poisson's ratio  $\nu = 0.3$  and a damping ratio of  $2.5\%$  to  $5\%$  were considered.

## ***5.2 Experimental results for displacements, seismic loads and failure mechanisms***

A set of key experimental measurements are presented in Figures 12 to 17, with reference to failure mechanisms, accelerations, dynamic and permanent displacements and bending moments, organised in sets of graphs suitable for comparisons. Most of the results presented here relate mainly to Configurations No1 and No3, since they exhibit yielding for similar

acceleration conditions, yet under different failure modes.

Observations on failure mechanisms can be made based on settlement profiles such as those depicted in Fig. 12, and from contour plots of acceleration distributions corresponding to the time instant of peak acceleration during active failure drawn in Fig. 13. The assumed failure mechanisms confirm the estimations based on the material properties, the stability analysis and the yield accelerations outlined in Tables 1 and 2 respectively, although this comparison is only indicative, as these are velocity characteristics not exactly coinciding with the corresponding stress characteristics [50]. Distinct failure mechanisms were observed only for transient earthquake loading, leading to large uniform deformations. Although there is no “rigid block” response in the retained soil mass, the experimental observations indicate that the earthquake excitation induces a more uniform acceleration distribution within the backfill over the harmonic loading, which corresponds to a more uniform stress field, as assumed in the pseudo-static analyses. The differences between backfill response to earthquake and harmonic loading have been discussed by Nakamura [13].

Time histories for accelerations, wall displacements and dynamic bending moments at the base of the wall stem are presented in Figs 14 - 17. Figures 14 and 15 pertain to harmonic loading (acceleration amplitudes of 0.19g and 0.23g). The response of each configuration is as expected, exhibiting a consistent, repeatable, behaviour with respect to yielding. A translational response mode is evident in Configuration No1 and a rocking one in Configuration No3, respectively. Sliding discontinuities are evident in the acceleration time histories of Configuration No1, at a critical acceleration compatible with that predicted by limit analysis considerations in Table 2. Note that the critical acceleration always increases as the wall toe penetrates the underlying soil layer, thus resulting to an increase in sliding resistance. This has also been observed in numerical simulations results [51]. On the other hand, Configuration No3 starts to rotate at initiation of yielding, without any evidence of sliding discontinuities on the recorded



accelerations. Evidence of rigid body rotation in the direction away from the backfill can be observed on the bending moment time history. Both configurations exhibit some rocking response, as a result of foundation rocking (which is more evident in Configuration No3) and possibly due to a pitch rotation of the shaking table itself.

Similar results for earthquake loading are presented in Figs 16 – 17. In this case, the input motion contains higher effective peak accelerations, but the number of important strong motion cycles (half cycle pulses) is only three. The sliding failure mode is, again, visible in Configuration No1, as is the bearing capacity failure in Configuration No3 (caused by the high eccentricities induced by the seismic thrust). An important observation about the failure modes is that the bearing capacity failure is more affected by the input acceleration level, whereas the behaviour of pure sliding mechanisms is mainly controlled by the duration of the strong ground motion, as known from sliding block theory [52]. Accordingly, rotational mechanisms appear to be more critical under strong ground shaking. Moreover, some rotational deformation is also observed in Configuration No1 for high acceleration level, revealing that the compliant base tends to induce local bearing capacity failure near the toe due to high stress concentration.

A noteworthy observation is that the bending moment at the base of the stem increases (positive  $\Delta M$ ) when the wall moves towards the backfill, that is for an acceleration level which is not critical for overall stability. On the other hand, during active conditions bending moment is minimised while displacement is maximum. Similar remarks have been made on the numerical simulations of a full scale cantilever retaining wall by Green et al. [51]. It appears that when the inertial action drives the wall towards the backfill, stresses increase towards the passive state, peak bending moments develop, and the backfill exhibits a stiffer behaviour.

### ***5.3 Interpretation of results in light of sliding block theory***

The ability to predict and control displacements under allowable limits for both sliding and

tilting is a key issue related to the performance based design of retaining walls. Although sliding block models (i.e. Richards & Elms [52]) are broadly applied, the evaluation of permanent rotation by means of equivalent rotational blocks (i.e. Zeng & Steedman [53]) is problematic due to rigid base assumptions.

Results for the incremental permanent wall displacement and rotation, together with corresponding eccentricities at the instant of failure, are presented in Figs 18 and 19, for Configurations No1 and No3, for both harmonic and seismic tests series. The corresponding critical acceleration values of Table 2, which are essential in the context of sliding block theory, are indicated on the graphs. It is worth mentioning that the critical accelerations that can induce uplift and overturning of the wall, in presence of a rigid base, are much higher (0.62g for Configuration No1 and 0.43g for Configuration No3) than the yield accelerations, so the overturning mechanisms are not feasible.

The following can be deduced from the graphs: First, the response of the systems with respect to translation and rotation is compatible with the predicted yield accelerations in Table 2. Second, the predictions of Richards & Elms [52] method overestimate the sliding displacements. This is evident in the case of Configuration No1, which is a mainly sliding mechanism, but not in the case of Configuration No3 where there is an underestimation of displacements for accelerations lower than critical. This is because response of Configuration No3 is mainly driven by the tilting failure mode, which is mobilised first. Third, both models exhibit a tendency for rotation at lower accelerations than those predicted by rotating block models, which arise from foundation yielding. In the particular case of Configuration No3, a rotation significantly exceeding the 1/500 limit specified by AASHTO is observed, accompanied by excessive settlement and bearing capacity failure. This rotation is related in both models, to eccentricities lower than the  $B/6$  limit. Fourth, Fig 17 suggests that for both Configurations, accelerations over a limit of 0.32g-0.35g cannot develop in the wall-soil

system. As a result, the eccentricities and rotations at yielding stop increasing proportionally to input acceleration. It appears that the plastic soil distortion under the wall toe, is beneficial for the system, by reducing the seismic forces transmitted to the foundation, thus preventing wall uplift and overturning.

#### ***5.4 Interpretation of dynamic bending moments***

Given that no direct measurements of earth pressures were made, some observations regarding dynamic stresses can be inferred from bending moment measurements on the wall stem. Note that the strain gauges performed adequately in recording the dynamic increment of bending moment,  $\Delta M$ , but not the static part.

In Fig. 20 an interpretation of peak measured dynamic bending moments is presented, based on simplified assumptions as to the variation of inertial forces and earth pressures behind the wall. It is assumed that the bending moments on the wall stem are generated by the inertial force  $F_w$ , due to the relative top-to-base acceleration  $A_6 - A_5$  [14] and the variation of the earth pressures  $\Delta P_E$  on the vertical virtual back. The latter is proportional to  $(a_w/g)\gamma z$  in the context of Wood's pseudostatic approach [54] under the assumption of linear variation of acceleration with depth, based on measurements of sensors A13 and A16. On the other hand, the inertial force acting on the soil mass over the footing slab (hatched area), which is moving in phase with the wall, is not taken into account [1, 18].

In Fig 21, envelopes of minimum and maximum bending moment profiles, as recorded from the strain gauges, are compared to the predictions of the theoretical approach for different harmonic (0.15g, 0.19g and 0.23g) and seismic (0.17g, 0.35g and 0.55g) loading for Configurations No1 and No3. A good agreement of measurements and predictions is evident in the graph, especially for the cases of seismic loading.

The contribution of the inertial force of the wall stem on the dynamic bending moment is found

to be small, between approximately 2.5% and 10% of the total dynamic moment, which is compatible to the findings of Al Atik & Sitar from centrifuge tests [14]. However, the inertia of the entire wall mass and the soil mass over the footing slab are important and have to be taken into account together with the active earth pressure on the virtual back determined by Eqns. (3) and (4), when the overall equilibrium of the soil-wall system is examined, as shown in Fig. 4. The increase in bending moments during wall displacement towards the backfill, is an indication that sizing the wall stem for active conditions is not conservative and different load combinations need to be employed [51]. Additional research is required to develop design recommendations.

## **6. Conclusions**

In the work at hand, results from 1-g shaking table tests on scale models of cantilever retaining walls were presented. The initial motivation of the study was the validation of recent stress limit analysis solutions for the seismic design of this type of retaining structures [21-23], in conjunction with the absence of specific design recommendations in seismic codes. Issues related to design and dynamic response of walls on a compliant base, were discussed. Both theoretical and experimental findings shed light on salient features of the problem. The main conclusions of the study are summarised below:

- 1) The proposed seismic Rankine analysis provides an exact solution for the pseudo-static seismic earth pressure acting under an acceleration-dependent inclination,  $\delta(\theta)$ , on the vertical virtual back of the wall, which is valid for the vast majority of cantilever walls supported by spread footings. The increase in thrust inclination with increasing seismic acceleration is a beneficial response mechanism which can be employed for reducing uncertainties and achieving rational and economic designs.
- 2) The experimental results confirm the predictions of the theoretical stress limit analysis,

with reference to the failure mechanisms and the critical yield accelerations of the system. Pseudo-static stability analysis performs adequately for both harmonic and seismic excitations. Earthquake loading leads to conditions which are closer to the assumptions of the pseudo-static analysis, namely the uniform distribution of acceleration and the “rigid block” response of the backfill.

- 3) The responses of the various experimental configurations examined, confirm the predictions of the stability analysis of the retaining walls in terms of an equivalent centrically-loaded footing and the relationship between wall tilting and bearing capacity failure. The validity of design recommendations in seismic codes (EC7, AASHTO LRFD) for avoiding excessive rotation is confirmed. The rotational mechanisms appear to be more sensitive to strong seismic shaking as compared to sliding mechanisms. In addition, an amount of tilting is observed in the majority of the tests and is attributed to plastic deformation/local bearing capacity failure under the wall toe, due to high eccentricities and inclination of soil reaction. The eccentricities are, nevertheless, smaller than the limit values specified by seismic codes. These findings highlight the importance of a proper design of walls founded on compliant base with respect to sliding and tilting.
- 4) Regarding seismic loads acting on the structure, it is shown that the soil thrust maximising the bending moment on the wall stem does not coincide with the critical active earth pressure, but develops when the wall is moving towards the backfill, due to the increased resistance and stiffness of soil, as the system is moving towards the “passive” state. This indicates that different load combinations need to be employed for the sizing of the wall stem and for the overall stability analysis of the wall against sliding and bearing capacity, which happens as the system moves towards the “active” state, away from the backfill. This observation is in agreement with the findings by Green *et*

*al.* [51]. Moreover, unlike the case of conventional gravity walls, inertial forces on the cantilever wall are less important for the overall stability compared to soil overburden, which mainly drive the behaviour of the system, and also have a small contribution to the dynamic bending moment, in agreement with the findings of Al Atik & Sitar [14] using centrifuge tests.

### **Acknowledgements**

The research leading to these results has received funding from the European Union Seventh Framework Programme (FP7/2007–2013) for access to the Bristol Laboratory for Advanced Dynamics Engineering (BLADE), University of Bristol, UK under grant agreement 227887 [SERIES]. The authors are also grateful to two anonymous reviewers whose comments improved the original manuscript.

### **References**

- [1] American Association of State Highway and Transportation Officials. LRFD Bridge Design Specifications. 6th ed. Washington DC: AASHTO; 2012.
- [2] EN 1997-1. Eurocode 7: Geotechnical Design, Part 1: General Rules. Bruxelles: CEN, E.C. for Standardization; 2004.
- [3] EN 1998-5. Eurocode 8: Design Provisions for Earthquake Resistance of Structures, Part 5: Foundations, Retaining Structures and Geotechnical Aspects. Bruxelles: CEN, E.C. for Standardization; 2004.
- [4] NEHRP 2009. Recommended Seismic Provisions for New Building and Other Structures. Washington DC: Federal Emergency Management Agency (FEMA P-750), Building Seismic Safety Council; 2009.

- [5] Shamsabadi A, Xu SY, Taciroglu E. Development of Improved Guidelines for Seismic Analysis and Design of Earth Retaining Structures. Caltrans Final Report No. CA13-2270. Los Angeles: UCLA; 2013.
- [6] Arias A, Sanchez-Sesma FJ, Ovando-Shelley E. A simplified elastic model for seismic analysis of earth-retaining structures with limited displacements. Proceedings of the International Conference on Recent Advances in Geotechnical Earthquake Engineering and Soil Dynamics, St. Louis 1981; 1: 235–40.
- [7] Veletsos AS, Younan AH. Dynamic soil pressures on rigid vertical walls. International Journal of Earthquake Engineering and Structural Dynamics 1994, 23: 275–301.
- [8] Theodorakopoulos DD, Chassiakos AP, Beskos DE. Dynamic Pressures on Rigid Cantilever Walls Retaining Poroelastic Soil Media. Part I: First Method of Solution. Soil Dynamics and Earthquake Engineering 2001; 21(4): 315–38.
- [9] Theodorakopoulos DD, Chassiakos AP, Beskos DE. Dynamic Pressures on Rigid Cantilever Walls Retaining Poroelastic Soil Media. Part I: First Method of Solution. Soil Dynamics and Earthquake Engineering 2001; 21(4): 339–64.
- [10] Ostadan F. Seismic soil pressure for building walls: an updated approach. Soil Dynamics and Earthquake Engineering 2005; 25(7–10): 785-93.
- [11] Kloukinas P, Langousis M, Mylonakis G. Simple wave solution for seismic earth pressures on nonyielding walls. Journal of Geotechnical and Geoenvironmental Engineering ASCE 2012; 138(12): 1514-19.
- [12] Watanabe K, Kobayashi Y, Touhata I, Macda T. Shaking-table tests on seismic earth pressure exerted on retaining wall model. Proc. 2<sup>nd</sup> Int. Conf. Earthquake Engineering; 1999.
- [13] Nakamura S. Reexamination of Mononobe-Okabe theory of gravity retaining walls using centrifuge model tests. Soils and Foundations 2006; 46(2): 135-46.

- [14] Al Atik L, Sitar N. Seismic earth pressures on cantilever retaining structures. *Journal of Geotechnical and Geoenvironmental Engineering ASCE* 2010; 136(10): 1324-33.
- [15] Wilson P, Elgamal A. Full scale bridge abutment passive earth pressure tests and calibrated models. *Proceedings of the 14th World Conference on Earthquake Engineering*. Beijing China; 2008.
- [16] Athanasopoulos-Zekkos A, Vlachakis VS, Athanasopoulos GA. Phasing issues in the seismic response of yielding, gravity-type earth retaining walls – Overview and results from a FEM study. *Soil Dynamics & Earthquake Engineering* 2013; 55: 59-70.
- [17] Seed HB, Whitman RV. *Design of Earth Retaining Structures for Dynamic Loads*. Proceedings, Specialty Conference on Lateral Stresses in the Ground and Design of Earth-Retaining Structures ASCE 1970. Ithaca, New York; 103-47.
- [18] Anderson DG, Martin GR, Lam IP, Wang JN. *Seismic Analysis and Design of Retaining Walls, Slopes and Embankments, and Buried Structures*. NCHRP Report 611. Washington DC: Transportation Research Board, National Research Council; 2008.
- [19] Shamsabadi A, Xu SY, Taciroglu E. A generalized log-spiral Rankine limit equilibrium model for seismic earth pressure analysis. *Soil Dynamics & Earthquake Engineering* 2013; 49: 197–209.
- [20] Brandenburg SJ, Mylonakis G, Stewart JP. Kinematic Framework for Evaluating Seismic Earth Pressures on Retaining Structures *Journal of Geotechnical and Geoenvironmental Engineering* 2015; 141. DOI: 10.1061/(ASCE)GT.1943-5606.0001312
- [21] Evangelista A, Scotto di Santolo A, Simonelli AL. Evaluation of pseudostatic active earth pressure coefficient of cantilever retaining walls. *Soil Dynamics and Earthquake Engineering* 2010; 30(11): 1119–28.
- [22] Scotto di Santolo A, Evangelista A. Dynamic active earth pressure on cantilever retaining walls. *Computers and Geotechnics* 2011, 38(8): 1041-51.



- [23] Kloukinas P, Mylonakis G. Rankine solution for seismic earth pressures on L – shaped retaining walls. 5ICEGE. Santiago Chile; 2011.
- [24] Kloukinas P, Penna A, Scotto di Santolo A, Bhattacharya S, Dietz M, Dihoru L, et al. Experimental Investigation of Dynamic Behaviour of Cantilever Retaining Walls. 2<sup>nd</sup> International Conference on Performance Based Design in Earthquake Geotechnical Engineering. Taormina Italy; 2012.
- [25] Scotto di Santolo A, Penna A, Kloukinas P, Bhattacharya S, Dietz M, Dihoru L, et al. Experimental Investigation of Dynamic Behaviour of Cantilever Retaining Walls. 15<sup>th</sup> World Conference on Earthquake Engineering. Lisbon; 2012.
- [26] Kloukinas P, Penna A, Scotto di Santolo A, Bhattacharya S, Dietz M, Dihoru L, et al. Experimental Investigation of Dynamic Behaviour of Cantilever Retaining Walls. Proceedings of the 4th ECCOMAS COMPDYN Thematic Conference on Computational Methods in Structural Dynamics and Earthquake Engineering. Kos Greece; 2013.
- [27] Kloukinas P, Penna A, Scotto di Santolo A, Bhattacharya S, Dietz M, Dihoru L, et al. Experimental Investigation of Dynamic Behaviour of Cantilever Retaining Walls. In: Ilki A, Fardis MN, editors. Seismic Evaluation and Rehabilitation of Structures, Geotechnical, Geological and Earthquake Engineering 26, DOI 10.1007/978-3-319-00458-7\_27, Switzerland: Springer International Publishing; 2014.
- [28] Lancellotta R. Lower-Bound Approach for Seismic Passive Earth Resistance. *Geotechnique* 2007; 57(3): 319-21.
- [29] Mylonakis G, Kloukinas P, Papantonopoulos C. An Alternative to the Mononobe–Okabe Equations for Seismic Earth Pressures. *Soil Dynamics and Earthquake Engineering* 2007; 27(10): 957-69.
- [30] Greco VR. Active earth thrust on cantilever walls in general conditions. *Soils and Foundations* 1999; 39(6): 65–78.

- [31] Huntington WC. Earth Pressures and Retaining Walls. NY: John Wiley and Sons; 1957.
- [32] Chu SC. Rankine analysis of active and passive pressures in dry sands. *Soils & Foundations* 1991; 31(4): 115 – 20.
- [33] Gazetas G, Garini E, Anastasopoulos I, Georgarakos T. Effects of Near-Fault Ground Shaking on Sliding Systems. *Journal of Geotechnical and Geoenvironmental Engineering ASCE* 2009; 135(12): 1906–21.
- [34] Greco VR. Stability of retaining walls against overturning. *Journal of Geotechnical & Geoenvironmental Engineering ASCE* 1997; 123(8): 778 – 80.
- [35] Dacoulas P, Gazetas G. Insight into seismic earth and water pressures against caisson quay walls. *Geotechnique* 2008; 58(2): 95-111.
- [36] Caltrans. California amendments to the AASHTO LRFD bridge design specifications 4th ed. Department of Transportation, State of California; 2011.
- [37] Butterfield R. On dimensioning the base of a traditional retaining wall. *Geotechnique Letters* 2012; 2: 25–8.
- [38] Marketos G, Madabhushi SPG. An investigation of the failure mechanism of a cantilever retaining wall under earthquake loading. *International Journal of Physical Modelling in Geotechnics* 2004; 4: 33-44.
- [39] Crewe AJ, Lings ML, Taylor CA, Yeung AK and Andrighetto R. Development of a Large Flexible Shear Stack for Testing Dry Sand and Simple Direct Foundations on a Shaking Table. In: Elnashai, editor. *European seismic design practice*. Rotterdam: Balkema; 1995.
- [40] Bhattacharya S, Lombardi D, Diloru L, Dietz MS, Crewe AJ, Taylor C. Role of seismic testing facilities in performance-based earthquake engineering. *Geological and Earthquake Engineering* 2012; 22: 135-58.
- [41] Younan AH, Veletsos AS. Dynamic response of flexible retaining walls. *Earthquake Engineering and Structural Dynamics* 2000; 29: 1815-44.

- [42] Cavallaro A, Maugeri M, Mazzarella R. Static and dynamic properties of Leighton Buzzard sand from laboratory tests. Proc. of 4<sup>th</sup> Int. Conf. on Recent Advances in Geotechnical Earthquake Engineering and Soil Dynamics and Symposium in Honour of Prof. WD Liam Finn. San Diego California; 2001.
- [43] Dietz MS and Muir Wood D. Shaking table evaluation of dynamic soil properties. Proceedings of the fourth international conference on earthquake geotechnical engineering. Thessaloniki Greece; 2007.
- [44] Lings M, Dietz M. The peak strength of sand steel interfaces and the role of dilation. Soils and Foundations 2005; 45(6): 1-14.
- [45] Dietz MS, Lings ML. Post peak strength of interfaces in a stress-dilatancy framework. Journal of Geotechnical and Geoenvironmental Engineering ASCE 2006; 132(11): 1474-84.
- [46] Muir Wood D, Crewe A, Taylor CA. Shaking table testing of geotechnical models. International Journal of Physical Modelling in Geotechnics 2002; 2: 1-13.
- [47] Hardin BO and Drenvich VP (1972) Shear modulus and damping in soils: design equations and curves. Journal of the Soils Mechanics and Foundation Division ASCE 1972; 98(SM7): 667-92.
- [48] Kramer SL. Geotechnical Earthquake Engineering. New Jersey: Prentice Hall; 1996.
- [49] Veletsos AS, Parikh VH, Younan AH. Dynamic response of a pair of walls retaining a viscoelastic solid. Earthquake Engineering and Structural Dynamics 1995; 24(12): 1587-89.
- [50] Chen WF and Liu XL. Limit Analysis in Soil Mechanics. Amsterdam: Elsevier; 1990.
- [51] Green RA, Olgun CG, Cameron WI (2008) Response and modeling of cantilever retaining walls subjected to seismic motions. Computer-Aided Civil and Infrastructure Engineering 2008; 23: 309–22.
- [52] Richards RJr, Elms DG. Seismic Behavior of Gravity Retaining Walls. Journal of the Geotechnical Engineering Division ASCE 1979; 105(GT4): 449-64.

- [53] Zeng X, Steedman RS. Rotating block method for seismic displacement of gravity walls. *Journal of Geotechnical and Geoenvironmental Engineering ASCE* 2000; 126: 709-17.
- [54] Wood JH. *Earthquake-Induced Soil Pressures on Structures*. EERL 73-05 Earthquake Engineering Research Laboratory, California Inst. of Technology, Pasadena CA; 1973.

## Figure captions

Figure 1. Problem parameters

Figure 2. Seismic stress tensor (a) and characteristics in Rankine wedge (b)

Figure 3. Variation of active thrust inclination on virtual vertical wall back  $\delta(0)$ , as function of horizontal seismic acceleration

Figure 4. Modified pseudostatic analysis of soil-wall system and wall stability in terms of equivalent centrically loaded footing analysis

Figure 5. Deviation of static Rankine (M-O with  $\delta = \beta$ ) and Coulomb (M-O with  $\delta = \delta_w = 2\phi/3$ ) analysis results, following the AASHTO recommendations, from the proposed exact seismic Rankine solution

Figure 6. Results for optimized wall geometry ( $b_1, b_2$ ) for various acceleration levels: a) Safety factor against sliding, b) Optimised base dimensions  $b_1$  and  $b_2$ , c) Eccentricity of soil reaction on footing, d) Increase in Safety Factors of optimised geometry, under gravitational loading

Figure 7. Geometry and instrumentation of the shaking table model (dimensions in mm)

Figure 8. Wall model geometry and positions of strain gauges (dimensions in mm)

Figure 9. Modified Sturmo (1980) acceleration input motion

Figure 10. Characteristic frequency response functions (FRF) of soil-wall system

Figure 11. Interpreted dynamic parameters of soil-wall model

Figure 12. Failure mechanisms back-calculated from measured surface settlements profile

Figure 13. Typical acceleration distributions in the soil during active failure conditions

Figure 14. Comparison of typical experimental results for Configurations No1 and No3 under sinusoidal - harmonic excitation of 0.19g with respect to: (a) wall accelerations, (b) wall displacements, (c) maximum dynamic moment  $\Delta M$  on the cantilever wall stem

Figure 15. Comparison of typical experimental results for Configurations No1 and No3 under sinusoidal - harmonic excitation of 0.23g with respect to: (a) wall accelerations, (b) wall displacements, (c) maximum dynamic moment  $\Delta M$  on the cantilever wall stem

Figure 16. Comparison of typical experimental results for Configurations No1 and No3 under seismic excitation of polarized PGA 0.35g with respect to: (a) wall accelerations, (b) wall displacements, (c) maximum dynamic moment  $\Delta M$  on the cantilever wall stem

Figure 17. Comparison of typical experimental results for Configurations No1 and No3 under seismic excitation of polarized PGA 0.55g with respect to: (a) wall accelerations, (b) wall displacements, (c) maximum dynamic moment  $\Delta M$  on the cantilever wall stem

Figure 18. Increments of permanent displacement and rotation and back-calculated load

eccentricities acting at the instance of failure, for Configuration No1 and No3 under harmonic excitation

Figure 19. Increments of permanent displacement and rotation and back-calculated load eccentricities at failure, for Configuration No1 and No3 under seismic excitation

Figure 20. Actions contributing to the dynamic bending moment on the stem of the cantilever wall

Figure 21. Variation of bending moments for Configurations No1 and No3, under harmonic and seismic loading of amplitudes 0.15g, 0.19g and 0.23g and 0.17g, 0.35g and 0.55g, respectively

# Figures

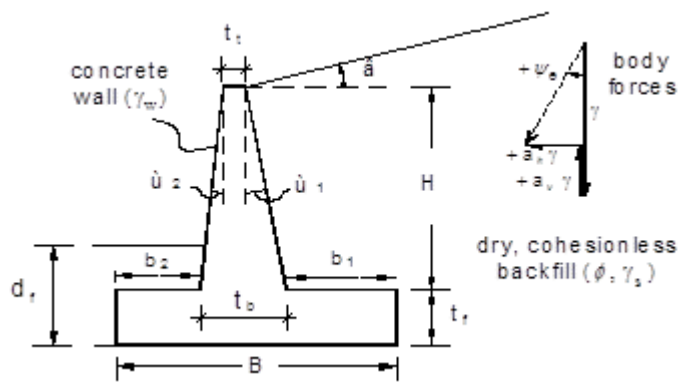


Figure 1

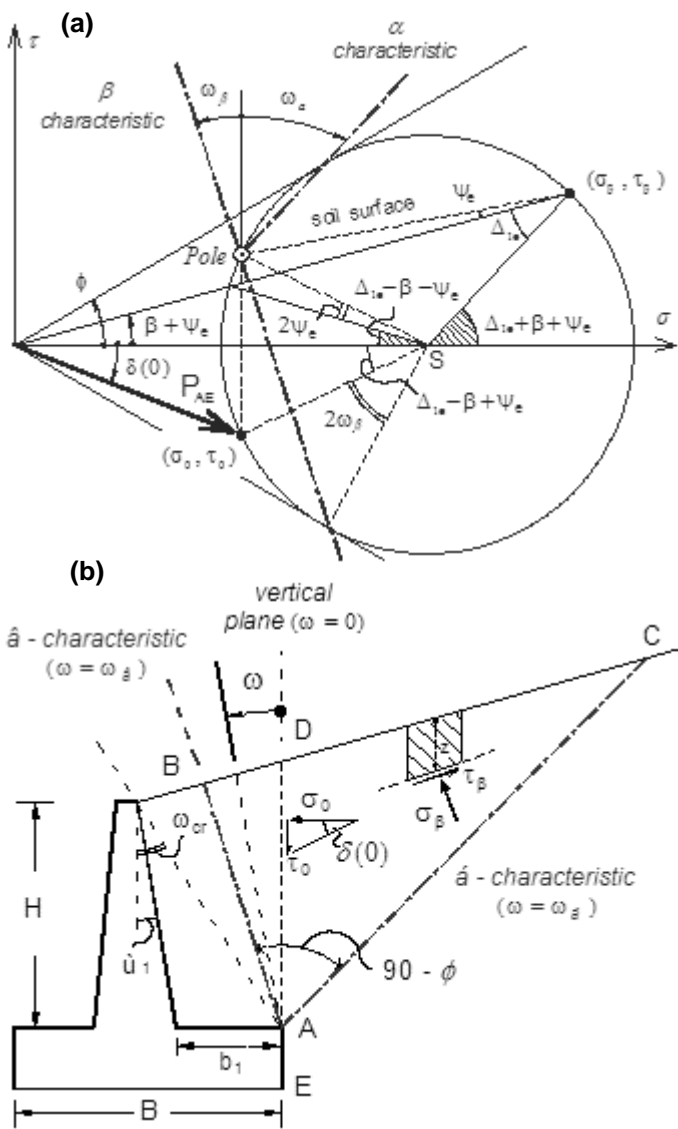


Figure 2

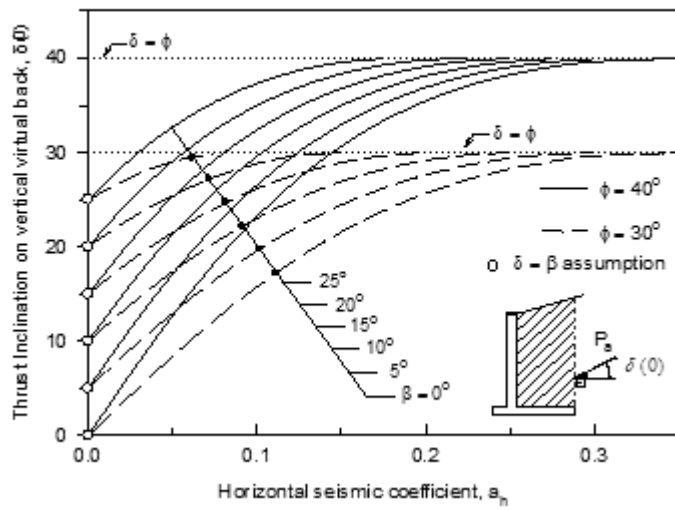


Figure 3

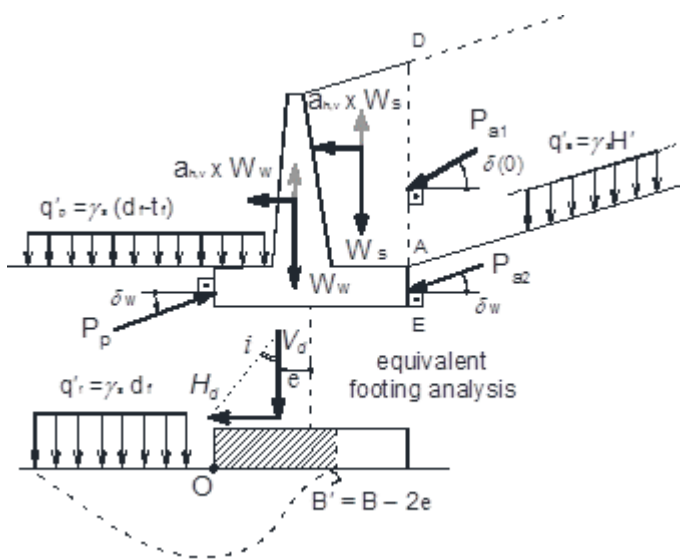


Figure 4



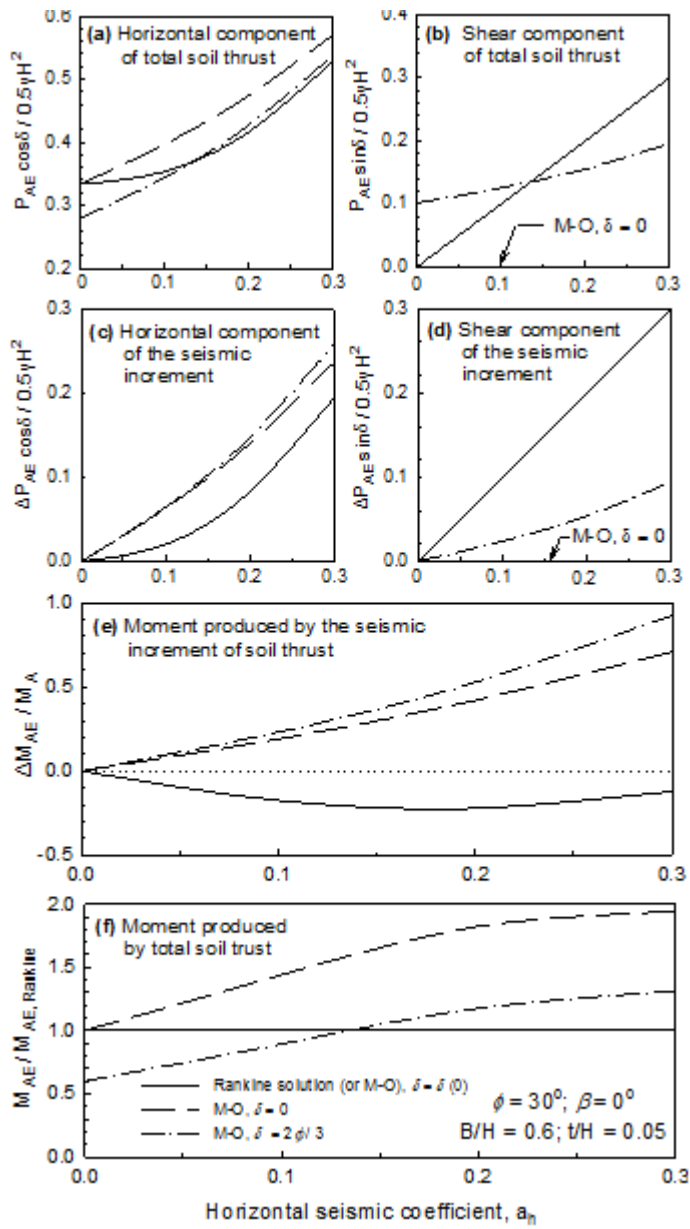


Figure 5

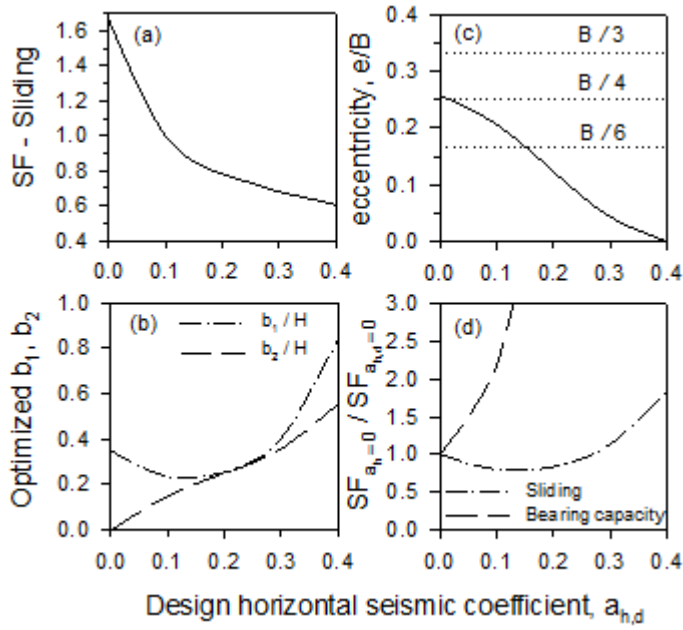


Figure 6

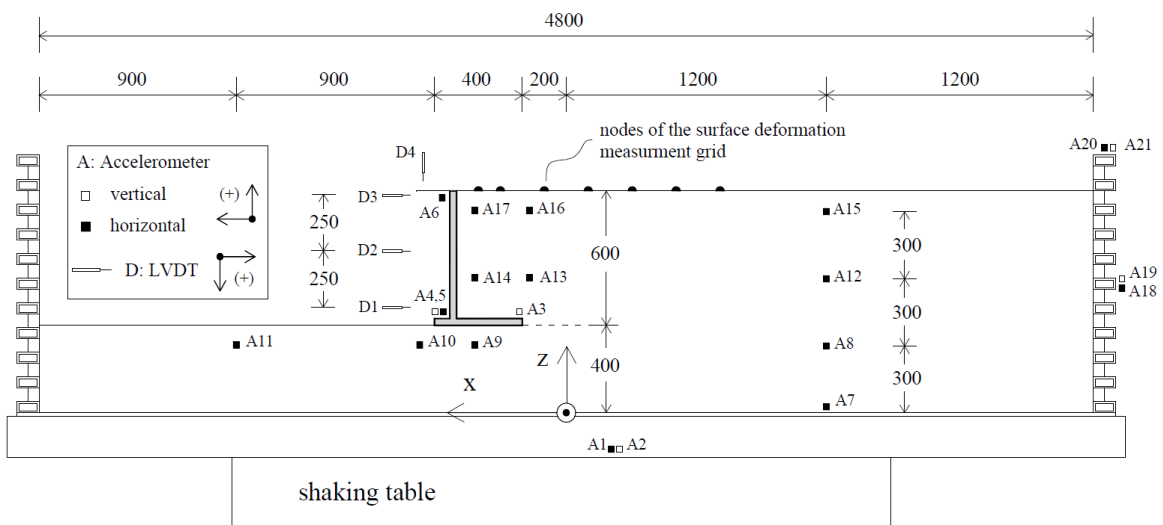


Figure 7

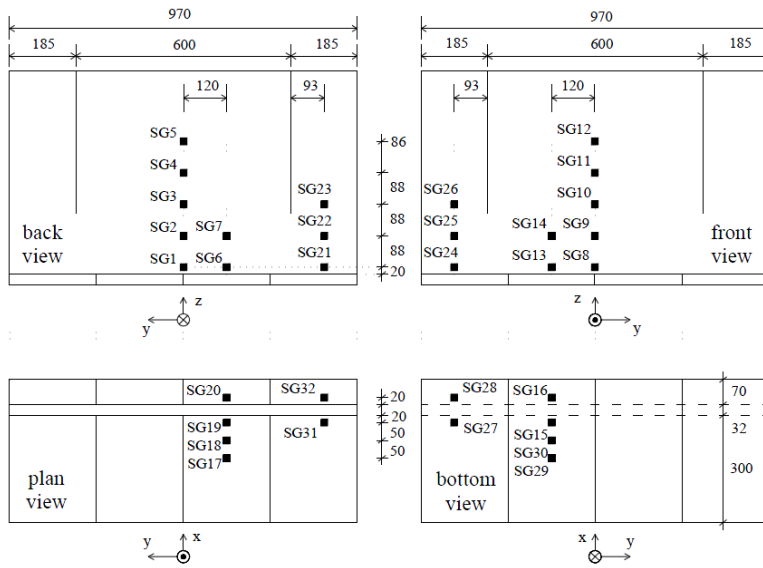


Figure 8

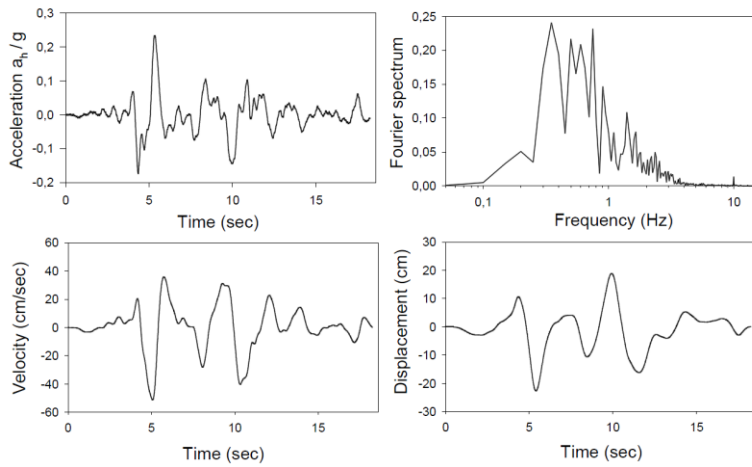


Figure 9

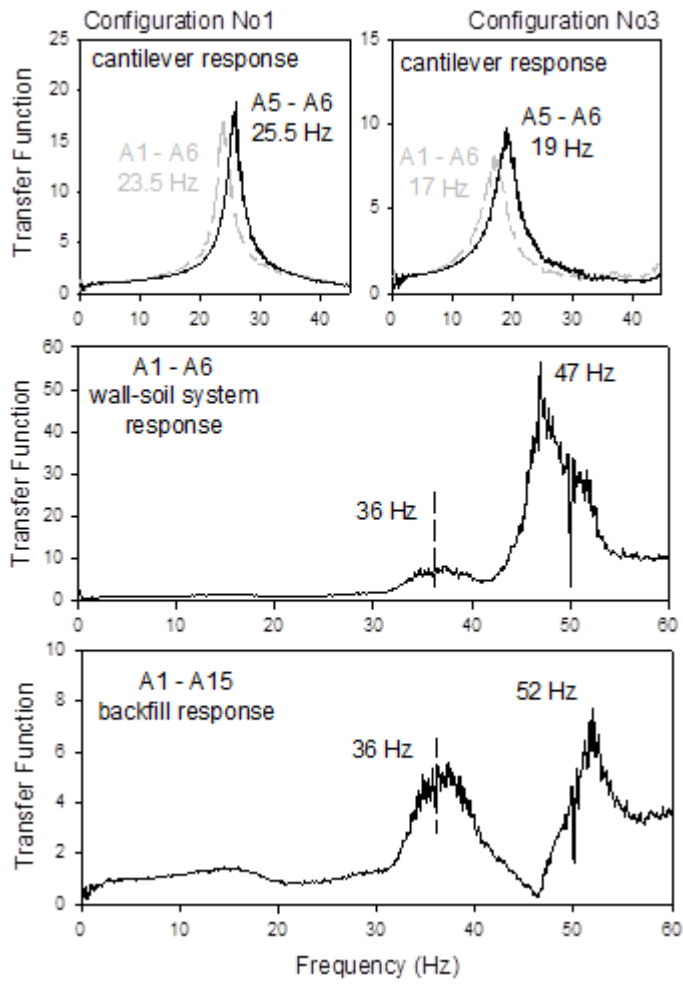


Figure 10

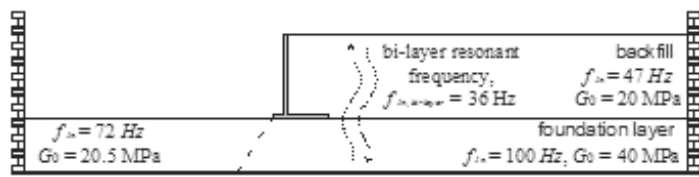


Figure 11

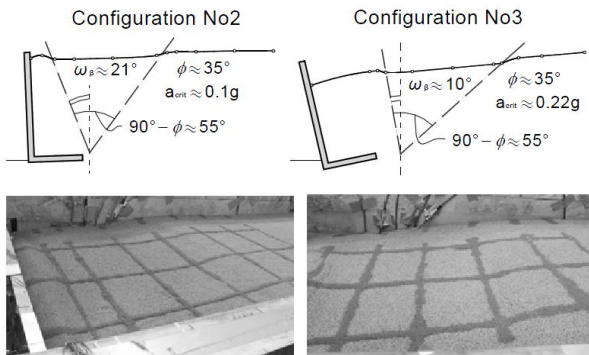


Figure 12

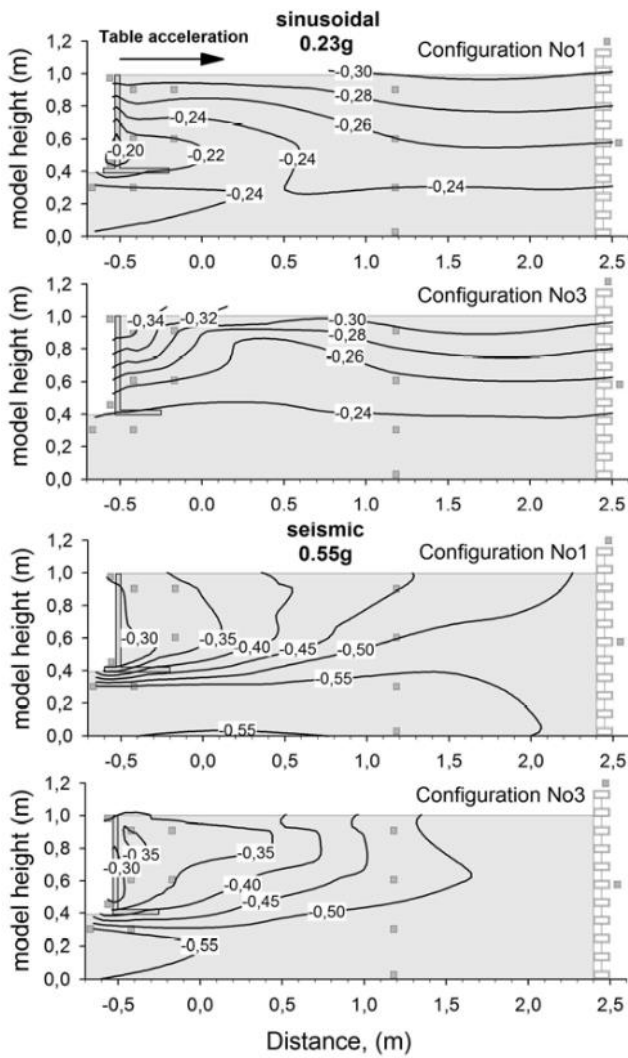


Figure 13

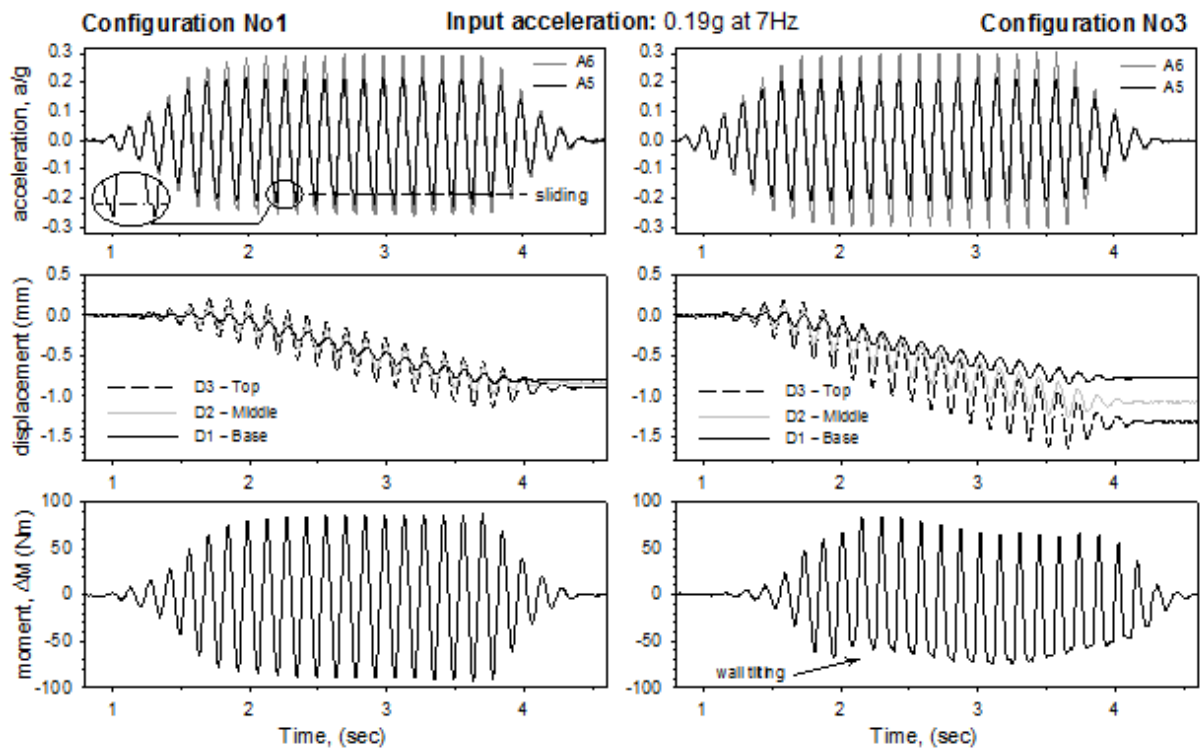


Figure 14

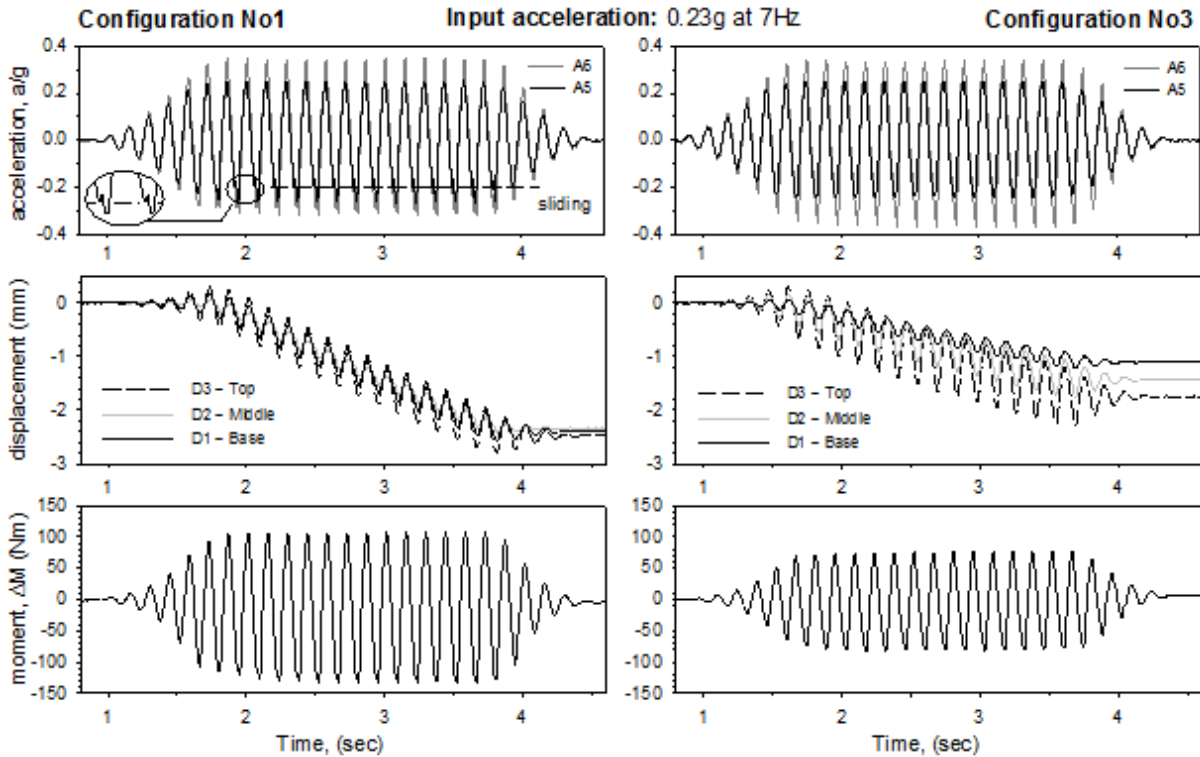


Figure 15

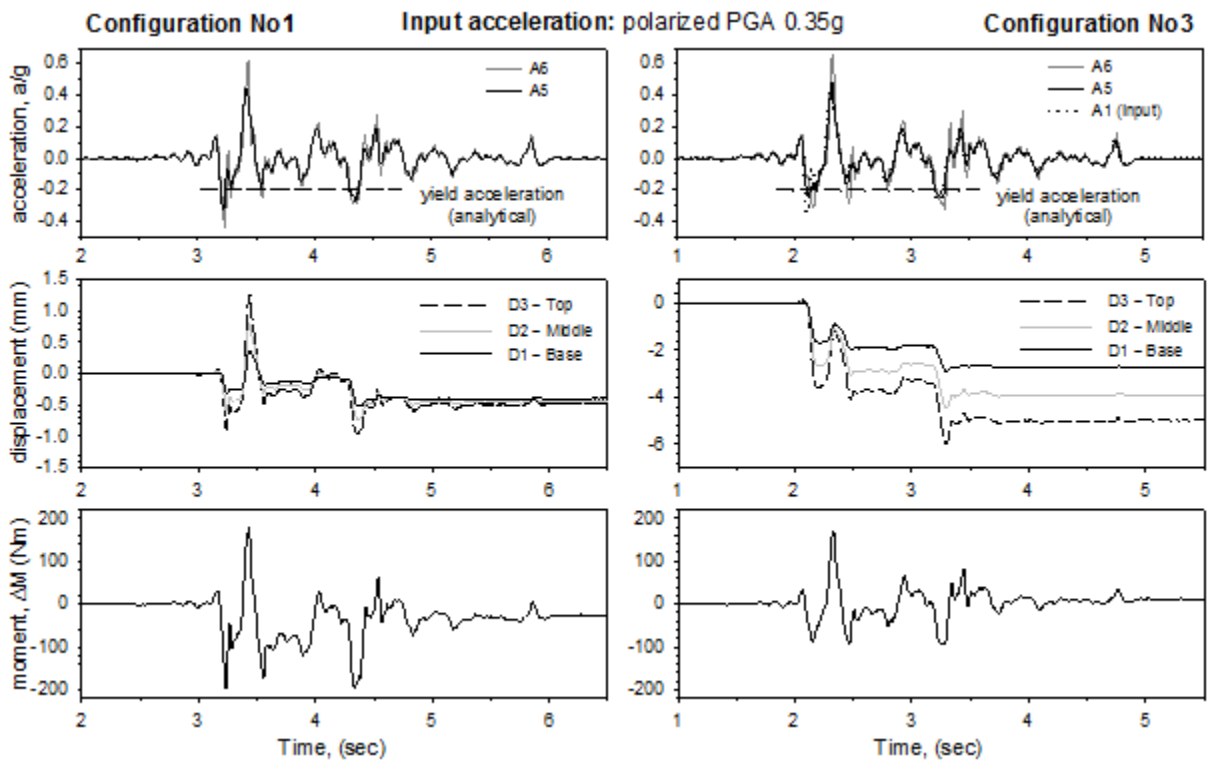


Figure 16

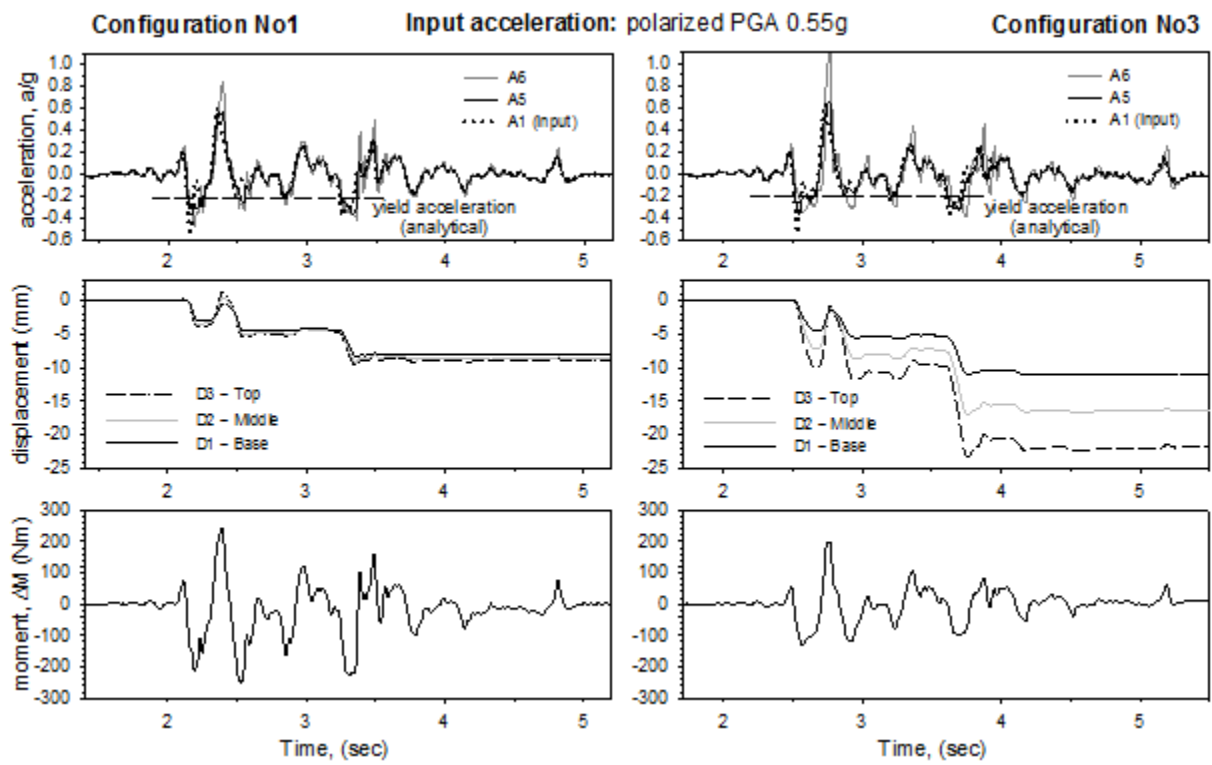


Figure 17

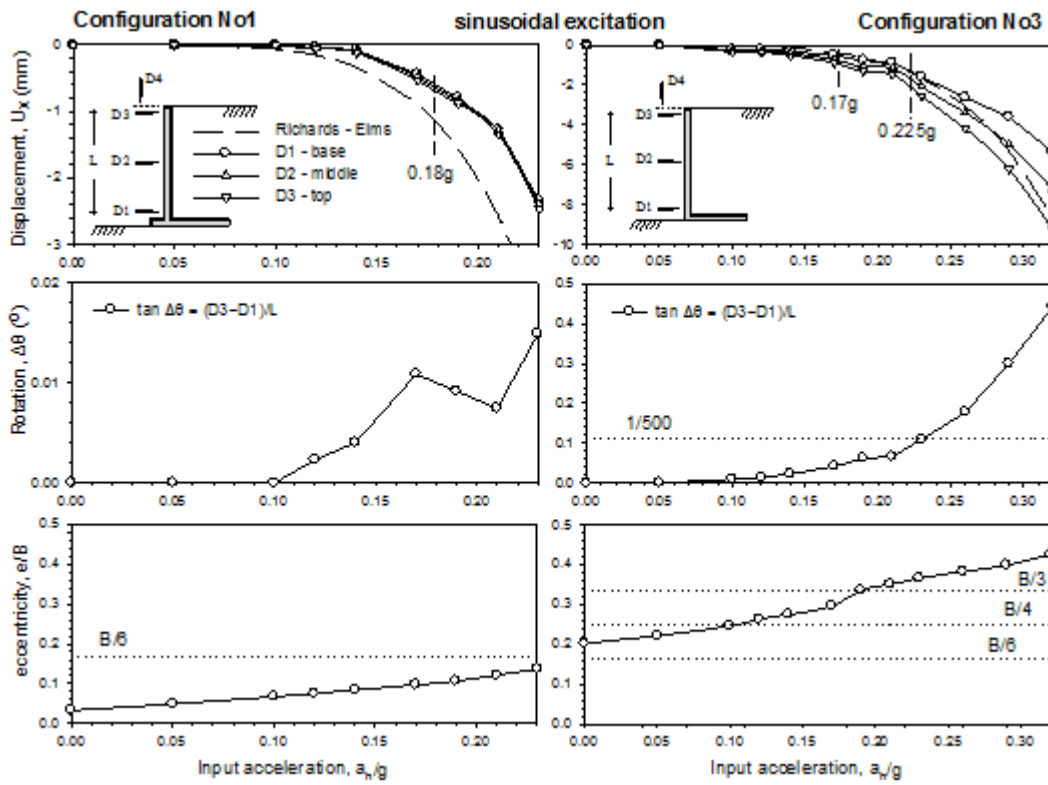


Figure 18

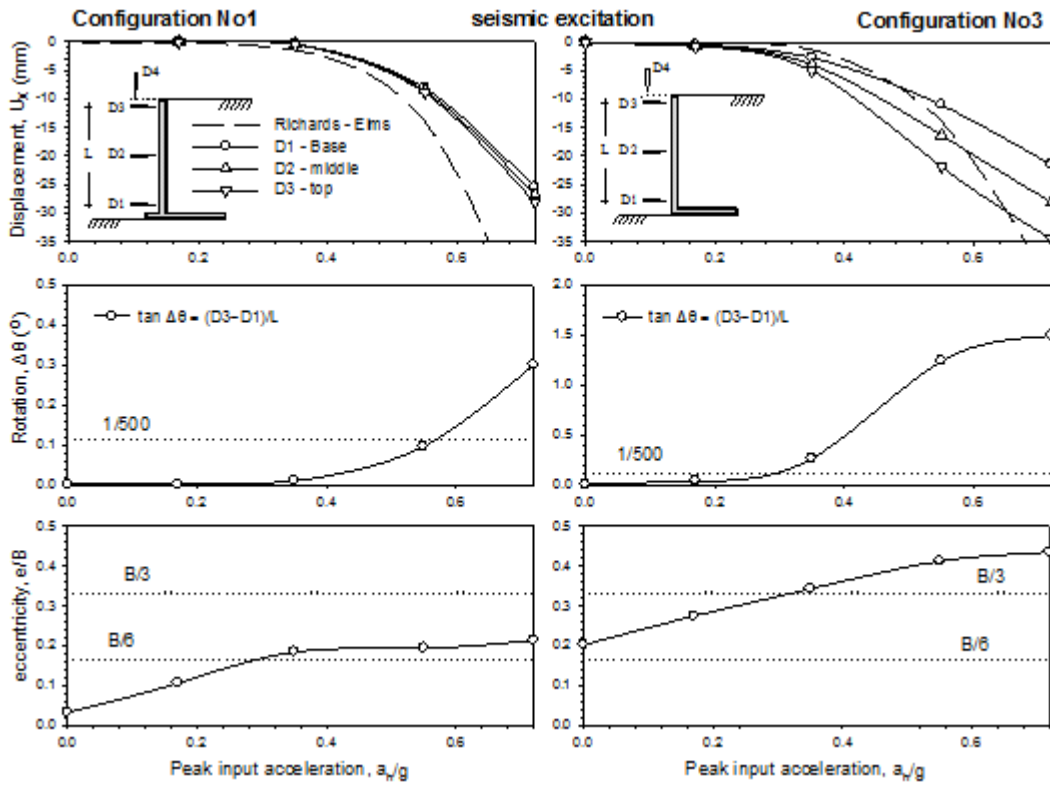


Figure 19



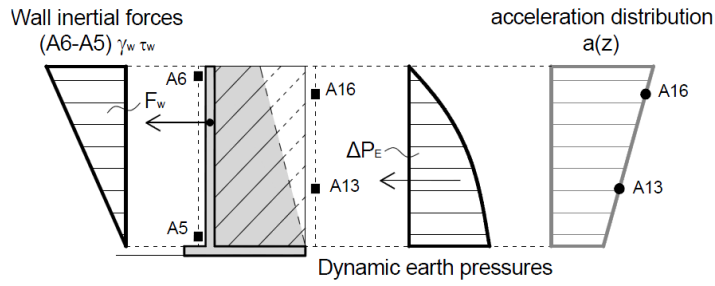


Figure 20

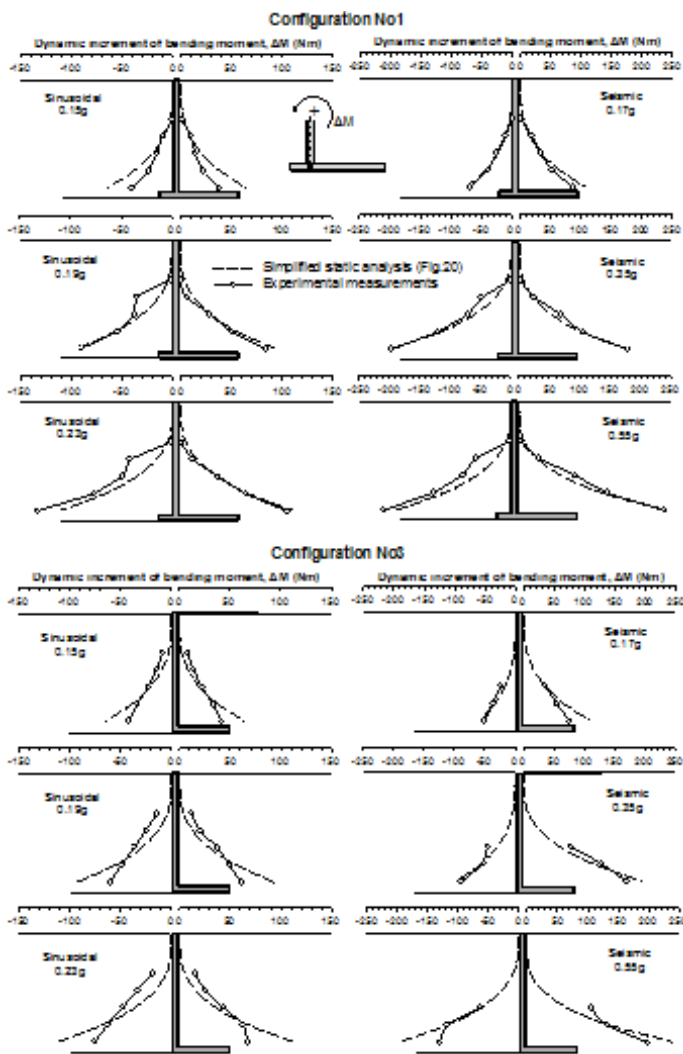


Figure 21

## Tables

**Table 1.** Soil properties

Soil layers	Voids ratio $e$	Relative density, $D_r$ (%)	Unit weight (kN/m <sup>3</sup> )
Foundation	0.61	60	16.14
Backfill	0.72	22	15.07

Leighton Buzzard 14 – 25 (Fraction B) sand properties:

$D_{min} = 0.6\text{mm}$ ,  $D_{max} = 1.18\text{ mm}$ ,  $D_{50} = 0.82\text{ mm}$ ,

$G_s = 2.64\text{ Mg/m}^3$ ,  $e_{min} = 0.486$ ,  $e_{max} = 0.78$

**Table 2.** Pseudostatic critical accelerations and associated safety factors (SF) with respect to sliding and bearing capacity.

Test configuration	Critical accel. $a_y$ , sliding	$SF_{bearing\ capacity}$ at $a_y$ , sliding	Critical accel. $a_y$ , bearing capacity	$SF_{sliding}$ at $a_y$ , bearing capacity
Configuration No1	0.18g	7.45	0.35g	0.68
Configuration No2	0.14g	1.46	0.17g	0.93
Configuration No3	0.23g	0.44	0.17g	1.14